

The effect of friction stir processing on the microstructure and mechanical properties of equal channel angular pressed 5052Al alloy sheet

N. Kumar · R. S. Mishra · C. S. Huskamp ·
K. K. Sankaran

Received: 12 January 2011 / Accepted: 21 March 2011 / Published online: 9 April 2011
© Springer Science+Business Media, LLC 2011

Abstract In this study, equal channel angular pressed (ECAP) 5052Al alloy sheet was friction stir processed (FSP). This was carried out to understand the effect of FSP on the microstructure and mechanical properties of the ECAP sheet. FSP led to further grain refinement and a tighter distribution of grains. Fraction of high-angle grain boundaries changed from 15% in ECAP condition to more than 70% after FSP. Although FSP caused lowering of yield strength (YS) and ultimate tensile strength (UTS), it resulted into a substantial improvement in uniform deformation region of the tensile sample (from 1.3% in as-received condition to 12.9% in FSP condition). Strain hardening rate (SHR) analysis showed lowering of recovery rate on FSP. A static grain growth model correctly predicted the average grain size obtained after FSP. Existing grain boundary, solid solution, and dislocation strengthening models were used to estimate the YS of 5052Al alloy in both the conditions. The strengthening model was able to predict the YS of the alloy in as-received and FSP conditions very well.

Introduction

In recent years, friction stir processing (FSP) has emerged as a potential severe plastic deformation technique (SPD) for grain refinement. FSP is a derivative of friction stir

welding (FSW) process which was developed in 1991 at TWI, UK by Thomas et al. [1]. FSP was introduced by Mishra et al. [2] in 1999 when they showed high-strain rate (HSR) superplasticity in a friction stir processed (FSP) 7075Al alloy. The details of this process can be found elsewhere [3, 4]. Subsequently, many researchers have reported the use of FSP as a grain refinement tool [5–11]. Su et al. [11] reported a grain size of 100 nm in a FSP 7075Al alloy. Rhodes et al. [10] obtained a grain size of 25–100 nm after FSP of 7050Al alloy. FSP causes not only a substantial reduction in the grain size but also results into an improvement in the fraction of high-angle grain boundaries (HAGBs) and uniform ductility [12].

Conventionally, processes such as equal channel angular pressing (ECAP) [13], high pressure torsion (HPT) [14], accumulative roll bonding (ARB) [15, 16], etc., have been used to refine the microstructure. Owing to limitations on the geometries which can be processed using these processes, it becomes necessary to subject such semi-finished products to further processing. For example, a cold-rolled (CR) sheet might undergo some joining process or some forming operation to give a material final shape. Sometime a material can be subjected to multiple processing techniques to take advantage of each processing technique. A secondary operation will result into a change in the microstructure and mechanical properties of an alloy. Zhu et al. [17] showed that the application of thermo-mechanical treatment to an ECAP UFG Ti resulted in improvement in mechanical properties of resulting Ti foils. Ti foils produced by the same thermo-mechanical treatment of a CG Ti showed inferior mechanical properties. Park et al. [18] reported increase in high-strain rate (HSR) superplastic elongation in a 5154Al alloy which was cold rolled after ECAP. Increase in HSR superplasticity was also reported by Nikulin et al. [19]. It was shown in their work

N. Kumar · R. S. Mishra (✉)
Department of Materials Science and Engineering, Missouri
University of Science and Technology, Rolla, MO 65409, USA
e-mail: rsmishra@mst.edu

C. S. Huskamp · K. K. Sankaran
Boeing Research and Technology, The Boeing Company,
St. Louis, MO 63166, USA

that equal channel angular extrusion followed by isothermal rolling at 250 °C resulted in HSR superplasticity. Akamatsu et al. [20] showed feasibility of producing superplastic sheets by combining ECAP and cold rolling of Al–Mg–Sc samples.

In this study ECAP has been combined with FSP. The primary goal of this study is to investigate the effect of FSP on ECAP 5052Al sheets. Combining both the processes (FSP and ECAP) might result in attractive combination of strength, ductility, and work hardening behavior. In this study, the effect of FSP on the microstructure has been studied in terms of distribution of grains and grain boundary misorientation. Mechanical properties have been compared in terms of change in uniaxial tensile strength, ductility and work hardening behavior of ECAP and FSP 5052Al alloy. An effort was made to predict the average grain size obtained after FSP by using a static grain growth model. Also, theoretical estimation of yield strength (YS) was carried out using existing grain boundary, solid solution, and dislocation strengthening models.

Experimental procedures

The ECAP of 5052Al sheet was carried-out at Monash University, Australia. The details of this process can be found elsewhere [21, 22]. The 5052Al sheet underwent three ECAP passes. The thickness of the ECAP sheet was ~ 1.6 mm. The nominal composition of the alloy was Al-2.5 wt% Mg-0.25 wt% Cr. It was friction stir processed (FSP) using a tool made of tool steel. The tool pin had step-spiral profile. The pin height and the shoulder diameter were 1.5 and 10.0 mm, respectively. The diameters of the pin near tool tip and pin root were 3.0 and 4.5 mm, respectively. A tool rotation rate of 400 rpm and a tool traverse speed of 3.4 mm/s were chosen to process the material. The tool tilt angle was 2.5° and plunge depth was 1.52 mm. The direction of tool traverse was in the direction of ECAP.

Grain size and its distribution in ECAP and FSP conditions were measured using electron backscattered diffraction (EBSD) microscopy. For ECAP material, EBSD was carried-out on a section parallel to the pressing direction. EBSD in FSP condition was done on transverse cross-section in the dynamically recrystallized region of the alloy. All the samples for EBSD were first mechanically polished using water-based diamond suspension up to 1 μm grit size, before final polishing with 0.02 μm colloidal silica suspension. EBSD was done on a FEI Helios NanoLab 600 FIB/FESEM fitted with an HKL Electron Backscatter Diffraction system. A step-size of 0.1 μm was chosen for OIM in both the conditions.

The strength of the ECAP and FSP 5052Al sheets were evaluated using mini-tensile testing at room temperature at an initial strain rate of $1 \times 10^{-3} \text{ s}^{-1}$. The gage orientation of the mini-tensile sample was transverse to the ECAP or FSP direction. Mini-tensile specimens had a gage length 1.3 mm, width 1.00 mm, and thickness 0.50 mm. Samples were polished using water-based diamond suspension up to 3 μm grit size before mini-tensile testing.

Results

Microstructure

The orientation imaging microscopy (OIM) images of the alloy in ECAP and FSP conditions are shown in Fig. 1. The OIM map is colored according to the projection of longitudinal direction (LD) in the inverse pole figure (IPF). The average grain size for ECAP condition was found to be $4.0 \pm 7.9 \mu\text{m}$. Since, some of the grains were as large as 48 μm, this caused standard deviation to be larger than the average grain size. The OIM micrograph corresponding to ECAP alloy is shown in Fig. 1a. White arrow in Fig. 1a indicates the ECAP direction. FSP caused grain-refinement of the alloys. After FSP the average grain size was $1.9 \pm 1.2 \mu\text{m}$. The OIM micrograph corresponding to FSP condition is shown in Fig. 1b. FSP caused not only reduction in the average grain size but also a tighter distribution of the grain size. Standard deviation from average value for ECAP alloy was 7.9 μm which on FSP reduced to 1.2 μm. The grain size distribution (GSD) histograms and corresponding cumulative GSD curves are shown in Fig. 2.

The misorientation angle distribution (MAD) is shown in Fig. 3. The MAD presented here is pixel-to-pixel misorientation frequency. It is evident that ECAP alloy had high amount (~85%) of low angle grain boundaries (LAGBs). In FSP condition, fraction of LAGBs changed to 30%. It is indicative of replacement of LAGBs with HAGBs during FSP. FSP also caused a reduction in dislocation density in the grain interior. Researchers have used local misorientation angle distribution (<2°) profile or grain average misorientation (GAM) [12] to assess the dislocation density inside a grain. A local MAD profile for this alloy in both the conditions (ECAP and FSP) is compared in Fig. 4. It shows that the local MAD profile corresponding to FSP alloy lies left to the profile of ECAP alloy. Local MAD was used to calculate GAM. The GAM values were found to be 0.55° and 0.32° in ECAP and FSP conditions, respectively, after taking measurement error of 0.3° into account [12]. A lower GAM value in FSP condition is indicative of low dislocation density in the grain interior.

Fig. 1 OIM images of 5052Al in **a** ECAP and **b** FSP. The white arrow in (**a**) is ECAP direction. Thick black lines are high-angle grain boundaries ($>15^\circ$) and gray thin lines in OIM images represent grain boundaries with misorientation 2° – 15°

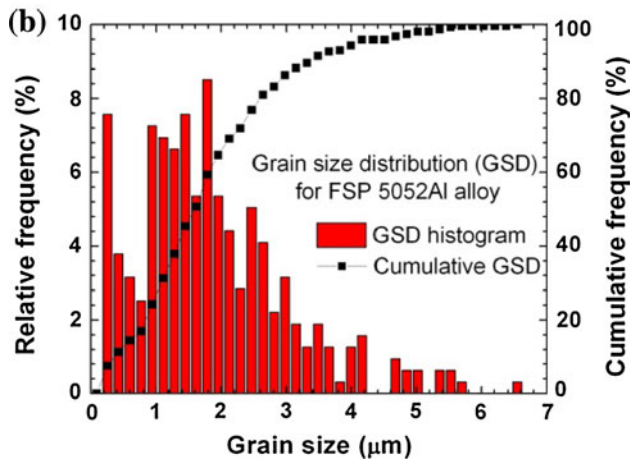
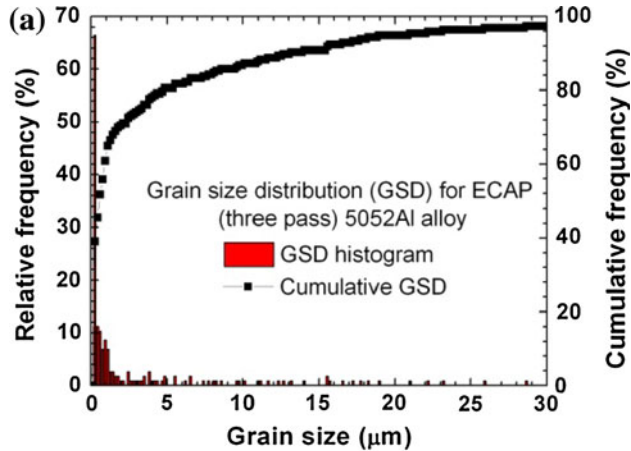
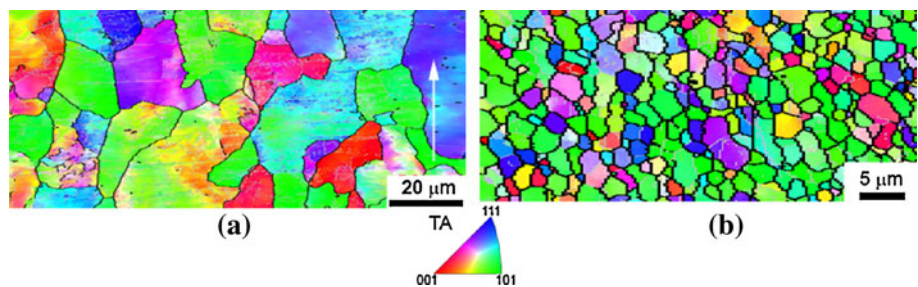


Fig. 2 Grain size distribution and corresponding cumulative curves of 5052Al alloy in **a** ECAP and **b** FSP conditions

Mechanical properties

The mini-tensile test results are shown in Fig. 5 and are summarized in Table 1. 5052Al alloy in ECAP condition had a YS and ultimate tensile strength (UTS) of 292 and 298 MPa, respectively. In this condition, this alloy showed a total elongation of 20%. Uniform elongation (UE) was just 1.3%. It indicates that most of the elongation was concentrated in post-necking region. It is clear also from the stress-strain curve for ECAP condition shown in Fig. 5. After FSP, there was a drop in both YS and UTS. In FSP

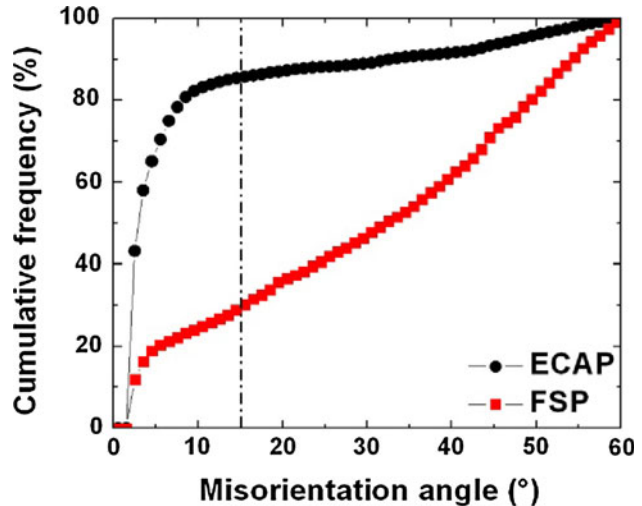


Fig. 3 Misorientation angle distribution of the 5052Al alloy in ECAP and FSP conditions

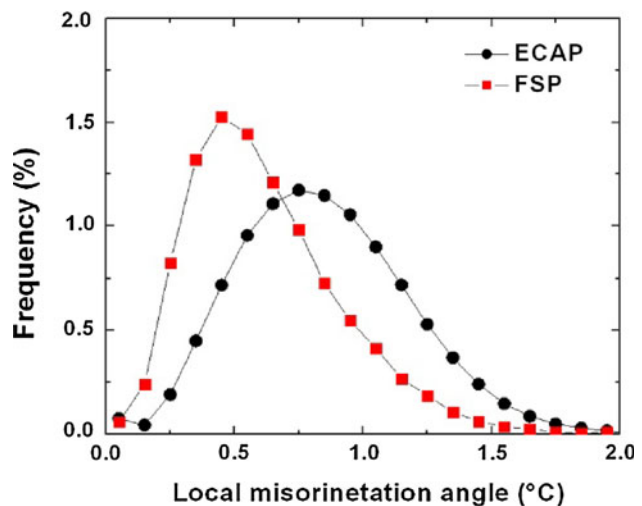


Fig. 4 Local misorientation angle distribution of 5052Al alloy in ECAP and FSP conditions

condition the alloy showed a YS of 192 MPa and UTS of 235 MPa. The total elongation was 22.5% and UE was 12.9%. After FSP, UE was $\sim 57\%$ of the total elongation undergone by the material. This was just 6.5% of total elongation in ECAP condition.

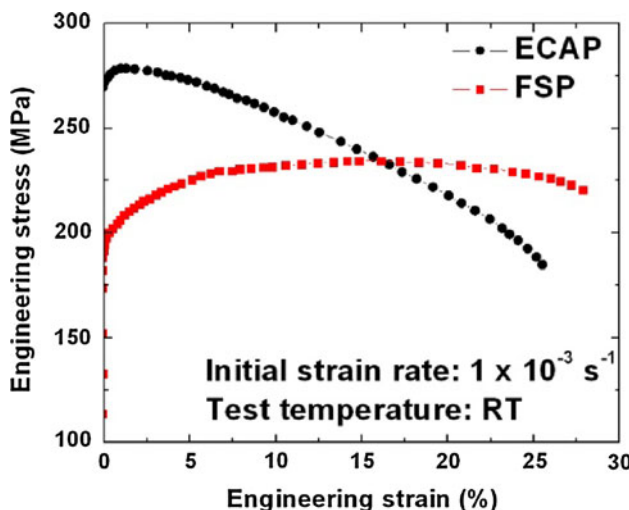


Fig. 5 Engineering stress–strain curves for ECAP and FSP conditions

Strain hardening rate (SHR) is reported in Fig. 6. It shows that rate of recovery is very high for the ECAP sample. Rate of recovery reduced after FSP. This is evident from the smaller slope of the solid line aligning with the linear portion of the curve as compared with the slope of the line for the curve representing ECAP sample. It should be noted that the post necking part of the stress–strain curve was not included for strain hardening rate calculation.

Discussion

Grain refinement and its growth during FSP

The average grain size listed in Table 2 and its distribution shown in Fig. 2 for FSP condition correspond to coarsened grains during the course of FSP. As mentioned earlier, Su et al. [11] and Rhodes et al. [10] demonstrated that FSP was capable of producing nano-sized grains if grain growth was arrested by deploying external cooling media. Grain refinement is subsequently followed by grain growth. The final average grain size depends on the peak temperature attained during processing and the type of alloy. For the same peak temperature, an alloy containing fine precipitates will show smaller grain size than that of single phase alloy. Absolute measurement of peak temperature attained

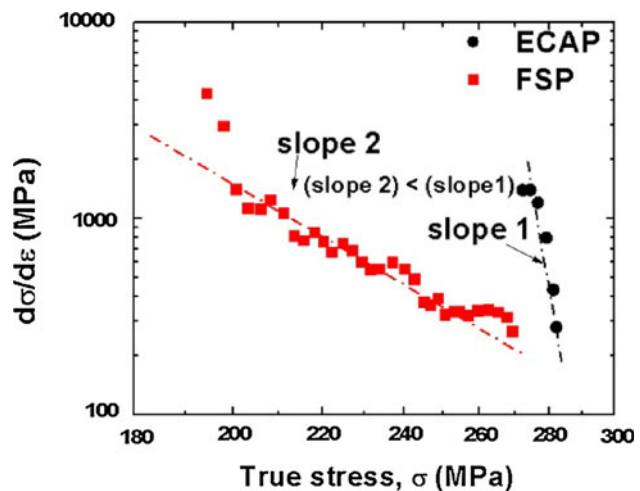


Fig. 6 Strain hardening rate variation as a function of true stress

Table 2 Average grain size, fraction of grain size less than 1 μm and fraction of HAGBs in ECAP and FSP conditions

	d_{av} (μm)	$d < 1 \mu\text{m}$	f_{HAGB}
ECAP	4.0 ± 7.9	70	15
FSP	1.9 ± 1.2	55	70

during FSP is not possible due to vigorous material movement in the nugget caused by the rotating and translating tool. Owing to inherent difficulty of measuring peak temperature in FSP, Arbegast and Hartley [23] obtained an empirical relationship for peak temperature and it is given as

$$\frac{T}{T_m} = K \left(\frac{\omega^2}{v \times 10^4} \right)^\alpha \quad (1)$$

where T_m is melting point of Al, K a constant ranging from 0.65 to 0.75, ω tool rotation rate in rpm, v traverse velocity in ipm, and α a constant ranging from 0.04 to 0.06. Taking K as 0.75 and α as 0.06, Eq. 1 gave T as 456 °C. Experimental study of temperature measurement has also shown peak temperature to be in the range of 400–500 °C [24–28] for aluminum alloys. Such a high temperature will induce grain growth of recrystallized grains.

Recrystallized grains on the trailing side of the tool go through grain growth process as the temperature is high enough to cause sufficient grain coarsening. Hillert [29] expressed growth rate of a uniform aggregate of grains of radius R (m), as

Table 1 Experimentally determined and theoretically estimated mechanical properties of ECAP and FSP materials

	YS (MPa)	UTS, (MPa)	% El	% UE	YS (MPa) (theoretical)	%error (exp. vs. theor.)
ECAP	292 ± 28	298 ± 27	20.0 ± 7.8	1.3 ± 0.2	293	+0.34
FSP	192 ± 4	235 ± 0.1	22.5 ± 7.5	12.9 ± 3.2	199	+3.65

Table 3 Values of the parameters used in Eq. 4 in the prediction of theoretical grain size

M_o (m ² /s) [30]	Q (kJ/mol) [31]	γ_b (J/m ²) [32]	t (s)	T (°C)
1×10^{-5}	90	0.324	10	450

$$\frac{dR}{dt} = \frac{M\gamma_{HAGB}}{4R} \quad (2)$$

Eq. 2 can be rewritten as $RdR = M\gamma_{HAGB}dt/4$. Integration of this between R and R_o gives an expression as

$$R^2 - R_o^2 = M\gamma_{HAGB}t/2 \quad (3)$$

Since, $R_o \ll R$,¹ Eq. 3 can be further simplified as

$$R \approx (M\gamma_{HAGB}t/2)^{1/2} \quad (4)$$

where M is the mobility of the grain boundary in m²/s, γ_{HAGB} energy of HAGB in J/m², and t time in seconds. M is a function of temperature and is generally expressed in the form of an Arrhenius equation as

$$M = M_o \exp\left(-\frac{Q}{RT}\right) \quad (5)$$

where M_o is mobility constant in m²/s, Q the activation energy of HAGB in J/mol, R the gas constant in J/(mol-K), and T the temperature in K. Table 3 lists various values used in the grain growth calculation. Substitution of the values of these parameters in Eq. 4 predicted average grain size to be 5.5 μm. In FSP condition average grain size was 1.9 μm. The maximum size of the grain detected by EBSD analysis was 6.7 μm. Hence, calculated grain size is within the range of grain size distribution and close to the experimentally obtained values. It should be noted that the calculated grain size represents an upper limit. In the calculation of the grain growth it has been assumed that grains experienced a temperature of 450 °C for 10 s (duration of the processing). In reality, this is not the case. A particular point in the wake of tool movement observes a continuously decreasing temperature. The decrease in temperature will cause decrease in mobility of grain boundaries. Also, in this calculation grain boundary mobility has been assumed to be a function of temperature only. But, it varies with grain boundary curvature and defect density also. When grains are very small, i.e., the curvature is very high, mobility of grain boundaries will be very high. As grains grow, curvature will reduce and so will grain boundary mobility. Therefore, the deviation of calculated grain size from the experimentally observed value is not surprising.

Yield strength of the alloy

Even in FSP condition 30% of the boundaries were LAGBs (Fig. 3). Hence, any discussion on the theoretical predictions of YS of the material should include contribution from LAGBs also. In a recent paper Kamikawa et al. [34] have demonstrated the significance of LAGBs (down to 2–3°) in the strengthening of ARB processed pure Al. General practice in modeling YS of a material is not to distinguish between high- and low-angle grain boundaries. In case of fully recrystallized materials, this assumption does not lead to a great deviation from the experimentally obtained values. But, for deformed materials, such assumption is not appropriate and generally leads to a large error between predicted and experimentally obtained values.

The YS of a material can be formulated on the basis of contribution from low- and high-angle grain boundaries, solid solution and dislocation as

$$\sigma_y = \sigma_{GB} + \sigma_{SS} + \sigma_D \quad (6)$$

where σ_y is the YS of the material, σ_{GB} the strength contribution from high- and low-angle grain boundaries, σ_{SS} the strengthening from solutes in solid solution, and σ_D the strengthening contribution due to dislocations. Following Hansen [35], strengthening contribution due to low- and high-angle grain boundaries is given as

$$\sigma_{GB} = \sigma_0 + \left[M\alpha G \sqrt{3b\theta_{LAB}(1-f)} + k\sqrt{f} \right] D_B^{-1/2} \quad (7)$$

where σ_0 is the lattice friction stress, k a constant, D_B the boundary spacing (defined as boundary misorientation ≥2°), M the Taylor's factor, α a material-dependent constant, G the shear modulus, b the Burgers vector, θ_{LAB} average of LAGB misorientations, and f fraction of HAGBs. Contributions because of solid solution and dislocations are given as

$$\sigma_{SS} = AC^\beta \quad (8)$$

$$\sigma_D = M\alpha G b \rho^{1/2} \quad (9)$$

In Eq. 8 [36], A is a constant equal to 13.8 MPa/(wt%)^β, C is solute content in wt%, and β is a constant equal to 1.14. In Eq. 9 ρ is the dislocation density. Substituting Eqs. 7–9 in Eq. 6 and simplifying it, the expression of YS is found to be as

$$\begin{aligned} \sigma_y = \sigma_0 &+ \left[M\alpha G \sqrt{3b\theta_{LAB}(1-f)} + k\sqrt{f} \right] D_B^{-1/2} + AC^\beta \\ &+ M\alpha G b \rho^{1/2} \end{aligned} \quad (10)$$

Table 4 lists the values of various parameters used in Eq. 10. Dislocation density was calculated using GAM values which was calculated using local misorientation

¹ As mentioned in the introduction section, during FSP grains as small as 25 nm can be obtained. But because of grain growth during processing commonly observed grain size is greater than 1 μm. Hence, this inequality holds good.

Table 4 Parameters used in Eq. 10 for the theoretical estimation of YS in ECAP and FSP conditions. The values of M , θ_{LAB} , f_{HAGB} , and D_B were obtained from EBSD data

	M	α [33]	G (GPa)	b (nm)	θ_{LAB} ($^{\circ}$) (2–15 $^{\circ}$)	f_{HAGB}	D_B (μm)	σ_o (MPa) [31]	k [31]
ECAP	2.25	0.3	26.2	0.286	4.09	0.15	0.545	20	0.04
FSP	2.25	0.3	26.2	0.286	5.38	0.71	1.025	20	0.04

distribution data (Fig. 4). The dislocation density calculation was made using following argument.

If all the dislocations are assumed to be part of a pile-up within a boundary spacing D_B , giving rise to a misorientation across such pile-up equal to the GAM, misorientation across the pile-up can be given as

$$\text{GAM}(\text{rad}) \approx \theta = b/d \quad (11)$$

where d is the dislocations spacing in such pile-ups. Inverse of d gives the linear density of the dislocation in the pile-up. Areal density of the dislocation can be obtained dividing linear density by grain boundary spacing, D_B . Equation 11 gave rise to a dislocation density of $6.10 \times 10^{13} \text{ m}^{-2}$ and $1.86 \times 10^{13} \text{ m}^{-2}$ for ECAP and FSP conditions, respectively.

Using these values in Eq. 10, YS in as-received and FSP conditions were found to be 293 and 199 MPa, respectively. Experimentally determined values for as-received and FSP conditions were 292 and 192 MPa, respectively. Hence, Eq. 10 predicted the YS of ECAP and FSP material very well.

Strain hardening rate

Four stages of work hardening have been reported so far [37]. Stage III of work hardening is most relevant since it decides the rate of hardening and recovery. Characteristics of stage III of work hardening is a decreasing SHR as a function of stress or strain. Stage III is generally expressed mathematically using Voce equation [37] which is given as

$$\frac{d\sigma}{d\varepsilon} = \frac{\alpha G b k_1}{2} - \frac{k_2 \sigma}{2} \quad (12)$$

where k_1 is a constant and k_2 is twice of the slope of the strain hardening versus stress plot and is linked with the rate of recovery. First term on the right hand side of Eq. 12 is rate of dislocation storage term and second term gives rate of annihilation of dislocations. According to this equation as stress increases, there is a decrease in SHR of a material which is also observed experimentally. Figure 6 indicates that FSP caused lowering of the slope and hence resulted in a lower rate of recovery in FSP condition. The reason for lower recovery rate can be attributed to lower fraction of LAGBs (21%) in FSP condition. The fraction of LAGBs was 85% in ECAP condition. LAGBs have been found to be a potential sink for dislocations. Sun et al. [38]

has shown with the help of stress–strain curves that LAGBs can act as effective sink for dislocations. In a recent work, Kapoor et al. [12] showed that the rate of recovery decreased linearly as fraction of HAGBs increased.

Ductility

The total ductility of the alloy in ECAP and FSP conditions are almost same. But, FSP caused a significant shift in uniform ductility of ECAP 5052Al alloy. In ECAP condition this alloy showed a uniform elongation of 1.3% which changed to 12.9% on FSP. The reason for such a drastic change is the difference in grain boundary character in both conditions. Hung et al. [39] have shown that UFG Al having higher fraction of HAGBs gave rise to higher uniform strain in comparison to UFG Al with lower fraction of HAGBs. In another study on UFG Cu [40], higher uniform ductility was associated with higher fraction of HAGBs. Kapoor et al. [12] also found uniform ductility to be related to fraction of HAGBs. Joo et al. [41] have also indicated that the presence of higher fraction of HAGBs resulted into good tensile ductility.

As mentioned earlier, ECAP alloy contained 85% of LAGBs whereas it was only 21% in FSP condition. Assuming a lower boundary cut off angle of 2 $^{\circ}$, boundary spacing was $\sim 0.55 \mu\text{m}$ and $\sim 1.0 \mu\text{m}$ in ECAP and FSP conditions, respectively. Also, a lower dislocation density was found for FSP alloy by using GAM values. The combination of relatively lower dislocation density and lower fraction of LAGBs in FSP condition suggests that mean free path for the movement of dislocations is more than that of ECAP alloy. A large mean free path for the movement of dislocations will introduce higher plastic strain in the material. It will result into higher UE. Also, as mentioned earlier, LAGBs have been associated with higher recovery rate in a material. Since fraction of LAGBs is higher for ECAP alloy, rate of recovery will be higher in this alloy and this will lead to early onset of plastic instability. Figure 6 supports this argument. The linear portion of the curve is a measure of the rate of recovery. The slope in ECAP condition is higher which is indicative of a higher rate of recovery. Outcome of this study can be applied to joining of such sheets. Since FSP led to reduction in the strength of the alloy, it indicates that if such materials are joined together the welded region will have lower strength

than parent region. Although parent alloy has a very high strength, application of such structures will be dependent on the mechanical properties of the welded region. Hence, it calls for selection of different process parameters for FSP which will lead to relatively lower reduction in the strength in the processed zone.

Conclusions

- (I) Combining FSP with ECAP resulted in further refinement of grains. FSP also caused a narrow distribution of grain size range in the processed region.
- (II) FSP of ECAP sheet resulted into increase in HAGBs from 15% in ECAP condition to 71% in FSP condition.
- (III) FSP caused decrease of YS and UTS of the ECAP material while the UE increased significantly.
- (IV) Improvement in strain hardening behavior and lowering of rate of recovery were observed in FSP condition as compared to ECAP condition.

Acknowledgement The authors thank Dr. Peter Thomson, the designer of the sheet-ECAP facility, who is with the Department of Materials Engineering, Monash University, Australia, for the equal channel angular processing of AA5052 sheets.

References

1. Thomas WM, Nicholas ED, Needham JC, Murch MG, Smith PT, Dawes CJ (1995) EP0615480 EPS UK
2. Mishra RS, Mahoney MW, McFadden SX, Mara NA, Mukherjee AK (1999) *Scripta Mater* 42:163
3. Mishra RS, Ma ZY (2005) *Mater Sci Eng R Reports* 50:1
4. Mishra RS (2007) In: Mishra RS, Mahoney MW (eds) Friction stir welding and processing. ASM International, Materials Park, Ohio
5. Charit I, Mishra RS (2005) *Acta Mater* 53:4211
6. Mishra RS, Mahoney MW (2001) *Mater Sci Forum* 357–359:507
7. Ma ZY, Mishra RS (2005) *Scripta Mater* 53:75
8. Su J-Q, Nelson TW, Sterling CJ (2005) *Scripta Mater* 52:135
9. Kwon YJ, Saito N, Shigematsu I (2002) *J Mater Sci Lett* 21:1473
10. Rhodes CG, Mahoney MW, Bingel WH, Calabrese M (2003) *Scripta Mater* 48:1451
11. Su J-Q, Nelson TW, Sterling CJ (2003) *J Mater Res* 18:1757
12. Kapoor R, Kumar N, Mishra RS, Huskamp CS, Sankaran KK (2010) *Mater Sci Eng A* 527:5246
13. Valiev RZ, Langdon TG (2006) *Prog Mater Sci* 51:881
14. Zhilyaev AP, Langdon TG (2008) *Prog Mater Sci* 53:893
15. Saito Y, Utsunomiya H, Tsuji N, Sakai T (1999) *Acta Mater* 47:579
16. Tsuji N, Saito Y, Lee S-H, Minamino Y (2003) *Adv Eng Mater* 5:338
17. Zhu YT, Kolobov YR, Grabovetskaya GP, Stolyarov VV, Girssova NV, Valiev RZ (2003) *J Mater Res* 18:1011
18. Park K-T, Lee H-J, Lee CS, Nam WJ, Shin DH (2004) *Scripta Mater* 51:479
19. Nikulin I, Kaibyshev R, Sakai T (2005) *Mater Sci Eng A* 407:62
20. Akamatsu H, Fujinami T, Horita Z, Langdon TG (2001) *Scripta Mater* 44:759
21. Lapovok R, McKenzie PWJ, Thomson PF, Semiatin SL (2007) *J Mater Sci* 42:1649. doi:[10.1007/s10853-006-0967-x](https://doi.org/10.1007/s10853-006-0967-x)
22. Lapovok R, Timokhina I, McKenzie PWJ, O'Donnell R (2008) *J Mater Process Technol* 200:441
23. Arbegast WJ, Hartley PJ (1998) In: Proceedings of the 5th international conference on trends in welding research. Pine Mountain, p 541
24. Rhodes CG, Mahoney MW, Bingel WH, Spurling RA, Bampton CC (1997) *Scripta Mater* 36:69
25. Liu G, Murr LE, Niou CS, McClure JC, Vega FR (1997) *Scripta Mater* 37:355
26. Murr L, Liu G, McClure J (1997) *J Mater Sci Lett* 16:1801
27. Tang W, Guo X, McClure JC, Murr LE, Nunes A (1998) *J Mater Process Manuf Sci* 7:163
28. Hashimoto T, Jyogan S, Nakata K, Kim YG and Ushio M (1999) In: Proceedings of the first international symposium on friction stir welding. Thousand Oaks, California
29. Hillert M (1965) *Acta Metall* 13:227
30. Robson JD, Campbell L (2010) *Sci Technol Weld Join* 15:171
31. Wang J, Iwahashi Y, Horita Z, Furukawa M, Nemoto M, Valiev RZ, Langdon TG (1996) *Acta Mater* 44:2973
32. Murr LE (1975) Interfacial phenomena in metals and alloys. Addison-Wesley, Reading
33. Starink MJ, Qiao XG, Zhang J, Gao N (2009) *Acta Mater* 57:5796
34. Kamikawa N, Huang X, Tsuji N, Hansen N (2009) *Acta Mater* 57:4198
35. Hansen N (2004) *Scripta Mater* 51:801
36. Ryen Ø, Holmedal B, Nijs O, Nes E, Sjölander E, Ekström H-E (2006) *Metall Mater Trans A* 37:1999
37. Kocks UF, Mecking H (2003) *Prog Mater Sci* 48:171
38. Sun PL, Yu CY, Kao PW, Chang CP (2005) *Scripta Mater* 52:265
39. Hung PC, Sun PL, Yu CY, Kao PW, Chang CP (2005) *Scripta Mater* 53:647
40. Zhao YH, Bingert JF, Zhu YT, Liao XZ, Valiev RZ, Horita Z, Langdon TG, Zhou YZ, Lavernia EJ (2008) *Appl Phys Lett* 92:081903
41. Joo S-H, Yoon S, Lee C, Nam D, Hong S, Kim H (2010) *J Mater Sci* 45:4652. doi:[10.1007/s10853-010-4382-y](https://doi.org/10.1007/s10853-010-4382-y)